Available online at www.sciencedirect.com
ScienceDirect
Journal of Colloid and Interface Science 318 (2008) 103–109
JOURNAL OF Colloid and Interface Science
www.elsevier.com/locate/jcis

Characterization of Langmuir–Blodgett organoclay films using X-ray reflectivity and atomic force microscopy

Jaseung Koo [a,*], Seongchan Park [a], Sushil Satija [b], Aleksey Tikhonov [c,d], Jonathan C. Sokolov [a], Miriam H. Rafailovich [e,*], Tadanori Koga [e,*]

[a] *Department of Materials Science and Engineering, State University of New York at Stony Brook, Stony Brook, NY 11794-2275, USA*
[b] *Center for Neutron Research, National Institute of Standards and Technology, Gaithersburg, MD 20899, USA*
[c] *Consortium of Advanced Radiation Sources, University of Chicago, Chicago, IL 60637, USA*
[d] *Brookhaven National Laboratory, National Synchrotron Light Source, Beamline X19C, Upton, NY 11973, USA*
[e] *Chemical and Molecular Engineering Program, State University of New York at Stony Brook, Stony Brook, NY 11794-2275, USA*

Received 4 July 2007; accepted 18 September 2007

Available online 3 October 2007

Abstract

Monolayers of organoclay platelets were formed at the air/water interface using the Langmuir technique and were then investigated either by *in situ* or lifted onto Si wafers and studied *ex situ*, using X-ray reflectivity (XR) methods. The XR data showed that the surfactant molecules on the clay platelets formed a dense, self-assembled monolayer where the molecules were tilted at an angle of $35^\circ \pm 6^\circ$ from the normal to the dry clay surface. The surfactant layers only covered a fraction of the clay platelet surface area, where the fractional surface coverage for the three clays studied (C6A, C15A, and C20A) was found to be 0.90, 0.86, and 0.73, respectively. These values were significantly higher than those estimated from the cation exchange capacity (CEC) values. Rather than being uniformly distributed, the surfactant was clustered in patchy regions, indicating that the surface of the clay platelets had both polar and non-polar segments. This heterogeneity confirmed the hypothesis which was previously invoked to explain the distribution of the clay platelets in melt mixed homopolymer and polymer blend nanocomposites.

Keywords: Organoclay; Langmuir–Blodgett technique; X-ray reflectivity; Cation exchange capacity

1. Introduction

Clays, layered silicates, have received considerable attention because of their potential use in numerous technical applications, ranging from nanocomposite materials to biomedical and personal care products. These clays are unique in the sense that they consist of negatively charged aluminosilicate layers kept together with exchangeable interlayer cations. These enable the clays to undergo ion exchange which makes it possible to modify their surfaces by intercalation of a cationic surfactant into the interlayer spaces. Hence a large number of alkylammonium-modified layered silicates (organoclays) have been developed, which are now widely used to form a large variety of nanocomposite materials [1–4] with enhanced material properties [5–8]. For example, it was recently demonstrated that modified clays can act as powerful compatibilization agents of polymer blends [9,10] and behave in a synergistic manner with standard flame retardant formulations to render a large class of polymers self-extinguishing [5].

To achieve the remarkable enhancement of the mechanical and thermal properties, it was also demonstrated that the clays must be exfoliated in the polymer matrix [5–7]. The process of exfoliation is very complex, but there is general agreement that in order for it to occur, the silicate platelets must first be coated with surfactant in order to enable them to overcome strong ionic interactions. The next factor is the interaction between the polymer chains and the platelet surface and the degree of surface coverage by the surfactant which will determine whether the clays will be well dispersed or clustered within the polymer

* Corresponding authors.
E-mail addresses: jkoo@ic.sunysb.edu (J. Koo), mrafailovich@notes.cc.sunysb.edu (M.H. Rafailovich), tkoga@notes.cc.sunysb.edu (T. Koga).

0021-9797/$ – see front matter
doi:10.1016/j.jcis.2007.09.079

matrix. In order to determine whether a specific functionalized clay will exfoliate in a matrix it is useful to determine these parameters. Numerous methods exist, which can characterize the interaction between the polymer and the surfactant. On the other hand, very few techniques exist that can give an accurate determination of the amount of a surfactant coverage. Usually surfactants are added in excess, but only the amount actually grafted onto the clay is important. Unbound surfactants can cause other problems, such as combustibility or plasticization. Therefore it is important to accurately determine the amount of the coverage on the platelets. To measure the amount of surfactants in organoclay particles, thermogravimetric analysis (TGA) is generally used [11]. This technique, however, is not accurate since it cannot easily distinguish between surfactant molecules that are bound to the clay surface and excess unbound surfactant. Consequently, the surface coverage cannot be determined. Here we show that X-ray reflectivity can be a far more accurate technique to obtain this information. Using the Langmuir–Blodgett (LB) method, monolayer films were formed at the air/water interface from various commercial montmorillonite (MMT) clays (Southern Clay Cloisite groups) and X-ray reflectivity was performed both at the air/water interface and after lifting the films off the surface onto silicon wafers. The X-ray reflectivity method was proven to be a useful technique to determine the fractional surfactant surface coverage which can then be compared directly to the cationic exchange capacity (CEC) factor.

2. Experimental

Cloisite organoclays (C6A, C10A, C15A, and C20A) were purchased from the Southern Clay Company (USA) and used for these experiments. These organoclays consist of the mineral base (natural MMT) and an alkylammonium surfactant (dimethyldihydrogenated tallow (2M2HT) or dimethylbenzylhydrogenated tallow (2MBHT)). The specifications regarding the organoclay used are listed in Tables 1 and 2. The organoclays were dispersed in toluene (Aldrich, Missouri) at the concentration of 1 mg/ml after ultrasonication (Bransonic Co., Virginia) for 30 s. To obtain the clay monolayer, we applied the LB technique as demonstrated in other studies [12–15]. The organoclay suspended solution (100 μl) was spread uniformly on the deionized (DI) water subphase (total area (A) = 745 cm^2) in a Langmuir–Blodgett trough (KSV 5000, KSV Instruments, Inc., Connecticut) at room temperature. After the solvent evaporated, the film was compressed by a double-barrier control at a rate of 5 mm/min. Surface pressure/area (π–A) isotherms were monitored and recorded during the compression. The films were then vertically transferred onto hydrophobic silicon substrates at 2 mm/min, followed by rinsing with DI water gently and drying under the vacuum at 80 °C for overnight. Atomic force microscope (AFM) images were obtained with a Nanoscope IIIa (Digital Instruments, USA) in contact mode in air, by using a commercially available Si_2N_4 cantilever. Specular X-ray reflectivity (XR) measurements for the dry films were performed using the X10B beamline with the wavelength, $\lambda = 0.87$ Å, at the National Synchrotron Light Source of the Brookhaven National Laboratory (Upton, NY). The XR profiles were measured as a function of the scattering wave-vector transfer normal to the surface, q_z ($= 4\pi \sin\theta/\lambda$), where θ is an incident angle. *In situ* XR was also conducted with a Bruker AXS-D8 Advance diffractometer (Cu$K\alpha$ radiation, $\lambda = 1.54$ Å) after mounting the trough on the sample stage. The modeling and fitting of the reflectivity was carried out based on a hyperbolic-tangent function model density profile $\rho(z)$ perpendicular to the sample surface [16]. The physical quantities to fit the data are the thicknesses (d), the interfacial root-mean-square (rms) roughness (σ) and the electron density (ρ). The electron density of the bulk components [17] is listed in Table 1.

Table 1
Chemical compositions and density of organoclays

	Chemical formula	Density (g/ml)	ρ_{bulk} (e/Å^3)
MMT	$Na_{0.2}Ca_{0.1}Al_2Si_4O_{10}(OH)_2$	2.2	0.66
2M2HT	$[N(CH_3)_2R_2]^+Cl^-$ [a]	0.8	0.26
2MBHT	$[N(CH_3)_2(C_7H_7)R]^+Cl^-$ [a]	0.8	0.27
DI water	H_2O	1.0	0.34

[a] R is a hydrocarbon chain (65% $C_{18}H_{37}$:30% $C_{16}H_{33}$:5% $C_{14}H_{29}$).

Table 2
Characteristics of organoclays used in this study

	Mineral base	Surfactant	Surfactant concentration (meq/100 g clay)	Company
C6A	MMT	2M2HT	140	Southern Clay
C10A	MMT	2MBHT	125	Southern Clay
C15A	MMT	2M2HT	125	Southern Clay
C20A	MMT	2M2HT	95	Southern Clay

3. Results and discussion

The surface pressure, π (mN/m), vs area-mass density (m^2/g), which is obtained from calculation of total trough area divided by the mass of clay spread on the water subphase, is plotted in Fig. 1. As can be seen in the figure, there is an abrupt onset pressure at an area of 410 m^2/g for the C15A clay and the pressure starts to increase linearly up to ∼20 mN/m. At this pressure, the films can be considered to be at the onset of a monolayer formation at the air/water interface [18] as shown in the inset in Fig. 1. On further compressing of the surface, the slope of the curve tends to be steeper since the monolayer becomes rigid above this surface pressure. The monolayer collapses at $\pi = 50$ mN/m and the film can be seen, even by optical measurements, to buckle on the water subphase.

To prove the monolayer formation of C15A at 20 mN/m, we performed specular XR measurement at the air/water interface. Fig. 2 depicts the *in situ* XR data of C15A as a function of q_z. We normalize the reflectivity (R), divided by q_z^{-4} to compensate the Fresnel's equation (R_F) decay, since the contrast between the water subphase and clay particle is low. After this normalization, then, the oscillation can be more easily distinguished as shown in Fig. 2.

To analyze the reflectivity data, we employed a five-layer model, i.e., a water subphase, a bottom surfactant layer, clay, a top surfactant layer, and air. In Fig. 2, the symbols are the ex-

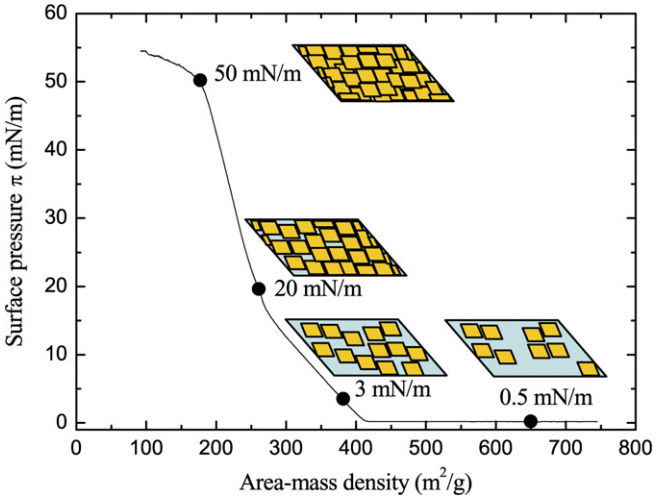

Fig. 1. π–A isotherm of C15A organoclay at the air/water interface.

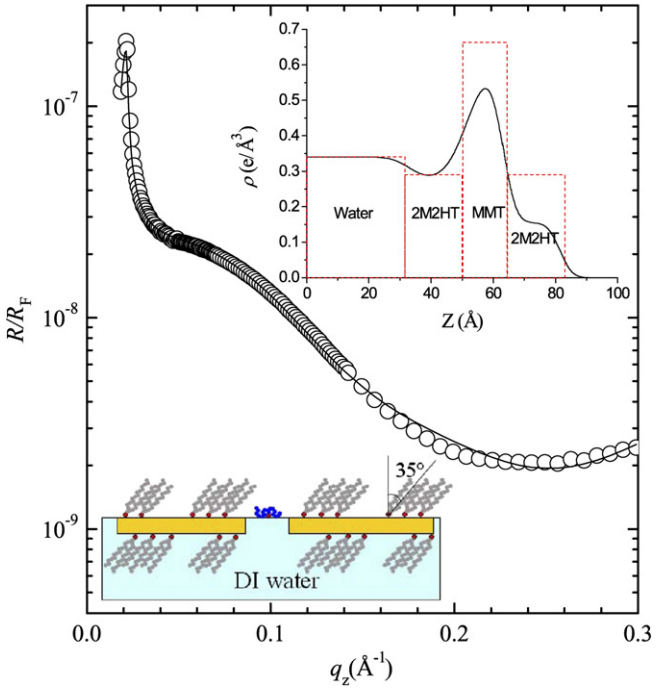

Fig. 2. *In situ* X-ray reflectivity profiles of C15A at $\pi = 20$ mN/m divided by the Fresnel's equation, q_z^{-4}. The solid lines are the best fit to the data. The insets depict the model of the organoclay monolayer at the air/water interface and the corresponding profile of the organoclay, where the dashed lines are the expected bulk value (ρ_{bulk}), assuming a sharp interface and a uniform coverage.

perimental data and the solid lines correspond to the best fits to the data on the basis of the model profiles shown as the inset in the figure. The electron density ($\rho = 2\pi\delta/\lambda^2\gamma_e$, where γ_e is the classical electron radius, equal to 2.814×10^{-5} Å, and δ is the dispersion coefficient [13]), thickness (d), roughness (σ), and coverage of organoclays obtained from the fits are listed in Table 3. From the table, we find that the thickness of the clay layer is 1.1 ± 0.3 nm, which allows us to confirm the formation of the single layer of organoclays at this surface pressure since the clay silicate layer is known to be approximately 1.2 nm thick according to the formal reports [19,20]. The thickness of the bottom 2M2HT layer is obtained to be 1.9 ± 0.3 nm which is nearly equal to that of the top surfactant layer. This surfactant length can then be compared with the known length of the surfactant molecules, 2.3 nm if the chain is fully extended. On the assumption that the surfactant layer is dense and the molecules are fully stretched, all the molecules are thought to be collectively tilted by an angle of $35° \pm 10°$ ($= \arccos(1.9/2.3)$) from the normal to the clay surface as shown in the schematic microscopic structure of the organoclays depicted in the inset of the figure.

We also used an atomic force microscopy (AFM) to confirm the monolayer formation of C15A as well as to observe the assembly process of the clays as a function of a surface pressure after transferring the film on the solid substrate. In Fig. 3a, we see that the organoclays form island domains on the water immediately after spreading. These islands with various sizes are widely separated on the water surface and therefore no surface pressure is built up at the water interface. Hence no true gas phase, as commonly observed with small molecule surfactants, exists. After further compression, these domains merge together into compressible structures (see Fig. 3b or the inset in Fig. 1) and eliminate the water phase gradually, thus the pressure starts to build rapidly. At $\pi = 20$ mN/m, the clays get closer with each other, and only a very small amount of free space can be found between the particles (see Fig. 3c or the inset in Fig. 1). As the film is compressed further up to 50 mN/m, the clay islands come into contact with each other, and a further decrease in the area is no longer possible (see Fig. 3d or the inset in Fig. 1).

Therefore, we spread each of the tested organoclays on the DI water and lifted them up on the hydrophobic silicon wafers at the surface pressure corresponding to the monolayer formation (C6A, C10A, C15A, and C20A at 18, 20, 20, and 20 mN/m, respectively), then measured X-ray reflectivity to understand the conformation of organoclay films in the direction normal to the surface. Fig. 4 depicts the reflectivity profiles of C6A, C10A, C15A, and C20A films on the silicon substrates as a function of q_z. As can be seen in the figure, distinct fringes, which are directly related to the layer thickness, are observed at the air/solid interface due to a good contrast of the X-ray scattering. The models used to fit the data are shown in Fig. 5 ((a) C6A, (b) C10A, (c) C15A, and (d) C20A) where the parameters to be fit are the thicknesses (d), the interfacial rms roughness (σ) and the electron density (ρ) of the surfactant layer adjacent to the silicon substrate, the clay layer, and the surfactant layer at the air interface. These parameters obtained from the best fits to the data are tabulated in Table 3. From the table, we find that, for the 2M2HT modified clays (namely C6A, C15A, and C20A), the thickness of the clay layer, and the top and bottom layers of 2M2HT are 1.1, 1.9, and 0.5 nm, respectively.

The sample surface coverage of each layer is obtained by measuring the electron density (ρ) and dividing it by the expected bulk value (ρ_{bulk}). Three layers, i.e. the clay layer, the top and bottom surfactant layers, are calculated. The results are also summarized in Table 3. The fractional density of the sili-

Table 3
The calculated coverage of organoclays from AFM images in Fig. 6 and X-ray reflectivity, and fitting parameters on the basis of the model profiles in Fig. 5

	π (mN/m)	Composition	AFM	X-ray reflectivity				
			$C \pm 0.05$	d (nm) ± 0.3	σ (nm) ± 0.2	ρ (e/Å^3) ± 0.02	$C \pm 0.03$	$C_{surf}/C_{clay} \pm 0.04$
C15A on the air/water interface	20	Bottom 2M2HT	·	1.9	1.3	0.29	0.65	0.82
		MMT	·	1.1	0.8	0.58	0.79	·
		Top 2M2HT	·	1.8	0.7	0.16	0.63	0.80
Dry C6A	18	Bottom 2M2HT	·	0.5	0.6	0.24	0.88	1.22
		MMT	0.73	1.0	0.7	0.47	0.72	·
		Top 2M2HT	·	2.0	1.1	0.18	0.65	0.90
Dry C10A	20	Bottom 2MBHT	·	0.5	0.5	0.13	0.47	0.69
		MMT	0.76	1.1	0.8	0.44	0.68	·
		Top 2MBHT	·	1.9	0.7	0.03	0.13	0.19
Dry C15A	20	Bottom 2M2HT	·	0.5	0.4	0.25	0.92	1.19
		MMT	0.80	1.0	0.8	0.50	0.77	·
		Top 2M2HT	·	1.9	0.8	0.18	0.66	0.86
Dry C20A	20	Bottom 2M2HT	·	0.5	0.5	0.25	0.92	1.24
		MMT	0.78	1.1	0.8	0.48	0.74	·
		Top 2M2HT	·	2.1	0.7	0.20	0.54	0.73

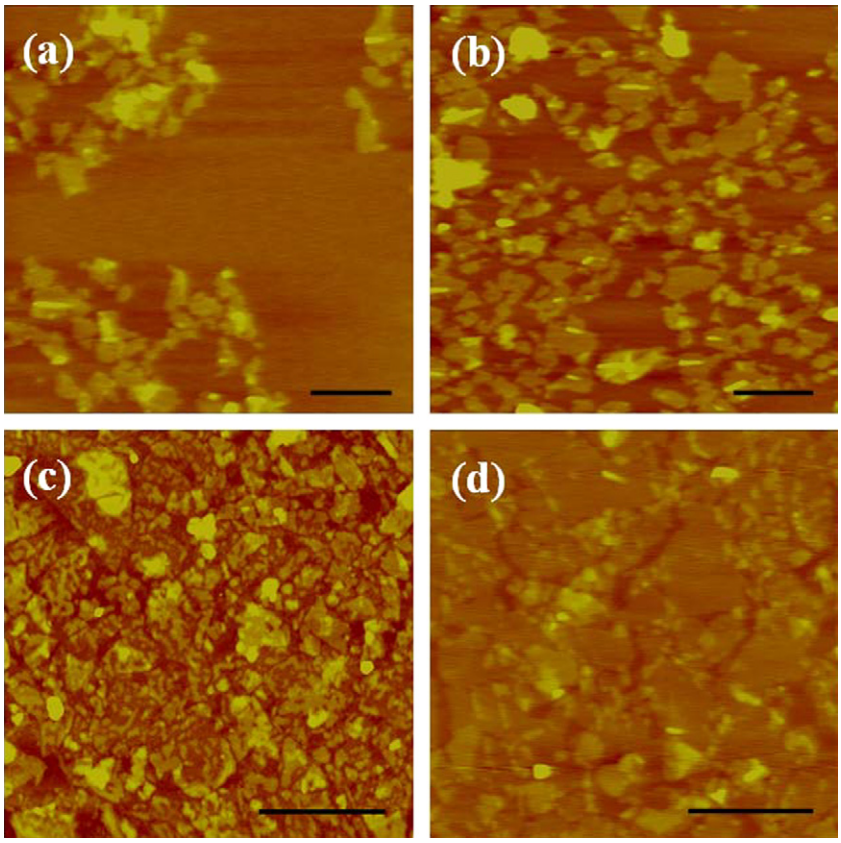

Fig. 3. AFM images of the films transferred onto hydrophobic Si wafers at the surface pressures of (a) 0.5, (b) 3, (c) 20, and (d) 50 mN/m. (The scale bars correspond to 1 μm.)

cate layer is interpreted as being due to a patchy surface with incomplete layer coverage. This is confirmed by scanning the silicon substrates after the clay films were lifted from air/water interface using scanning probe microscopy (SPM) (Fig. 6). From the figure we can see that none of the clays form a uniform film and in each case the surface coverage of the silicon wafer is partial. In order to compare with the reflectivity results, we then estimated the fractional surface coverage from the SPM images and tabulated them for each type of clay in Table 3. From the figure we see that the AFM images were in reasonable agreement with the X-ray reflectivity results. Any discrepancies were due to the fact that the AFM only probes a small area while the

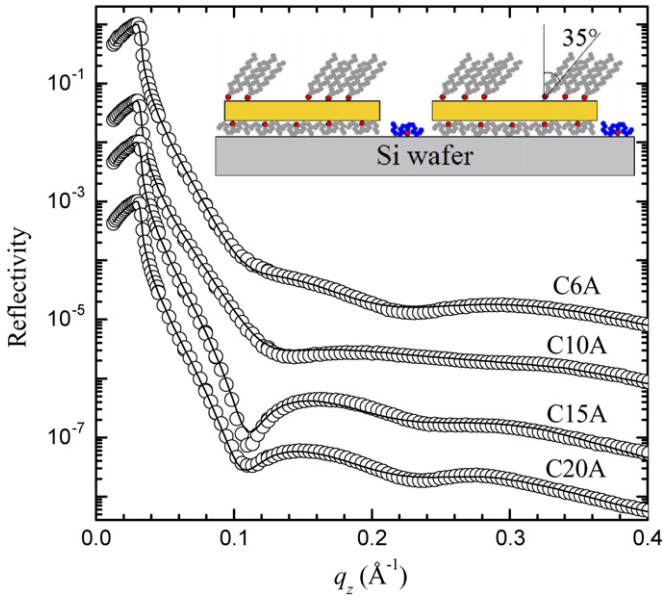

Fig. 4. X-ray reflectivity profiles of organoclays (C6A, C10A, C15A, and C20A) on silicon wafers. The solid lines are the best fits to the data. All curves are shifted for clarity. The inset depicts the model of the organoclay monolayer on the solid substrate.

incident X-ray beam averages over nearly the entire length of the sample.

The coverage of the surfactant on the clay, is calculated as follows. First we estimate the fraction of the Si surface covered by the clay platelets, C_{clay}, from the measured electron density corresponding to the clay layer, divided by the expected electron density, if the layer was intact. Then using the known values of the sample electron density, we calculate the fraction of the sample surface (Si+clay) covered by the surfactant. The ratio between the fraction of the surface covered by the surfactant, C_{surf}, divided by the fraction of the surface covered by the clay, C_{clay}, is the fractional coverage of the clay surface occupied by the surfactant. The results were tabulated in Table 3 and further compared with the surfactant concentration provided in the manufacturer's reference data [21].

When the clays are functionalized via ion exchange, the maximum uptake or CEC for Cloisite type clays is 92 meq/100 g. Yet, most organoclays have surfactant concentrations that are much higher, namely 140, 125, and 95 meq/100 g for C6A, C15A, and C20A, respectively, as can be seen in Table 2. Gelfer et al. [11] used small angle X-ray scattering (SAXS) and TGA to measure the actual weight percent of surfactants on clays. They found that the 2M2HT content in organ-

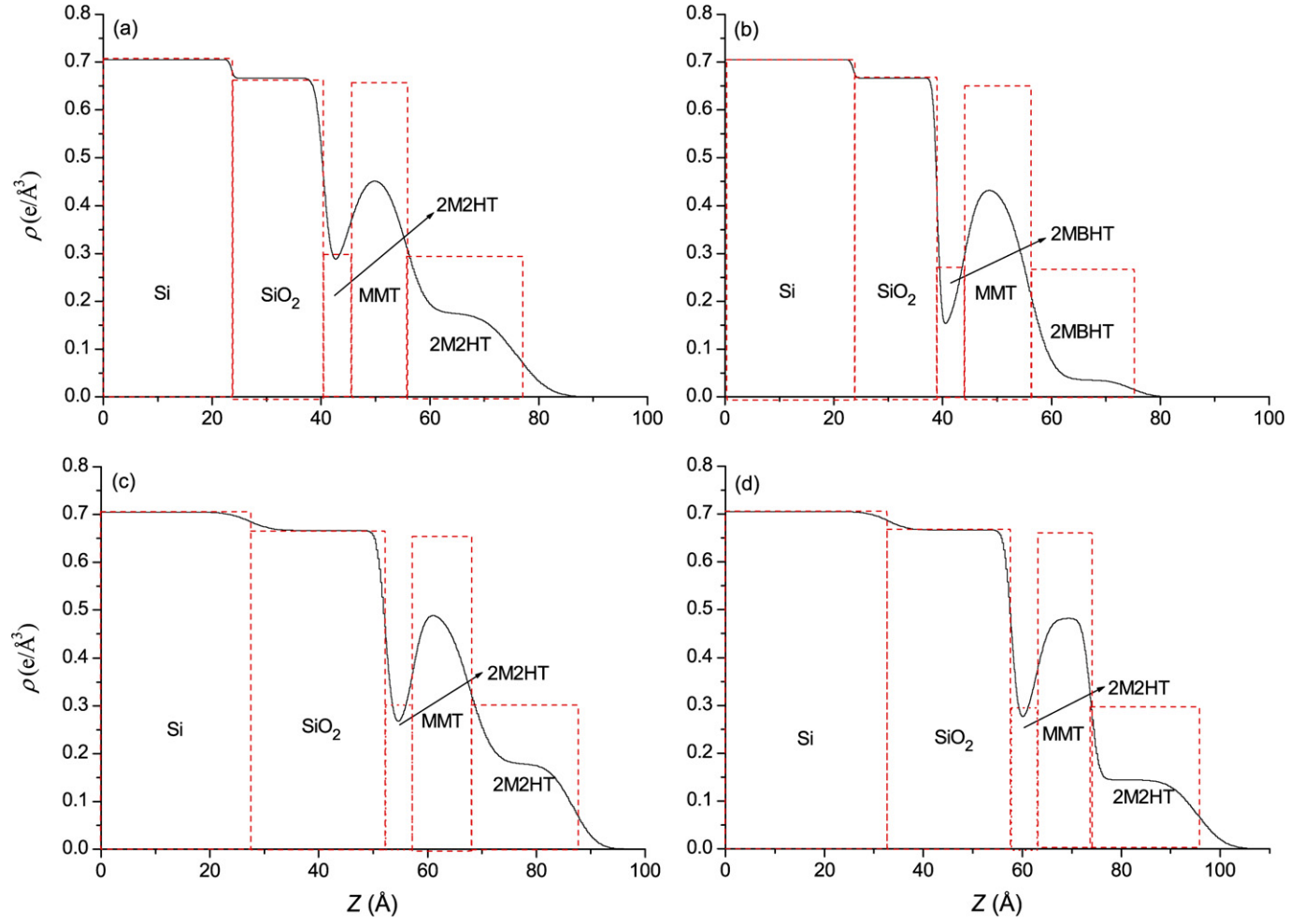

Fig. 5. Electron density profiles of the LB films of (a) C6A, (b) C10A, (c) C15A, (d) C20A on the silicon substrates. The dashed lines are the expected bulk value (ρ_{bulk}), assuming a sharp interface and a uniform coverage.

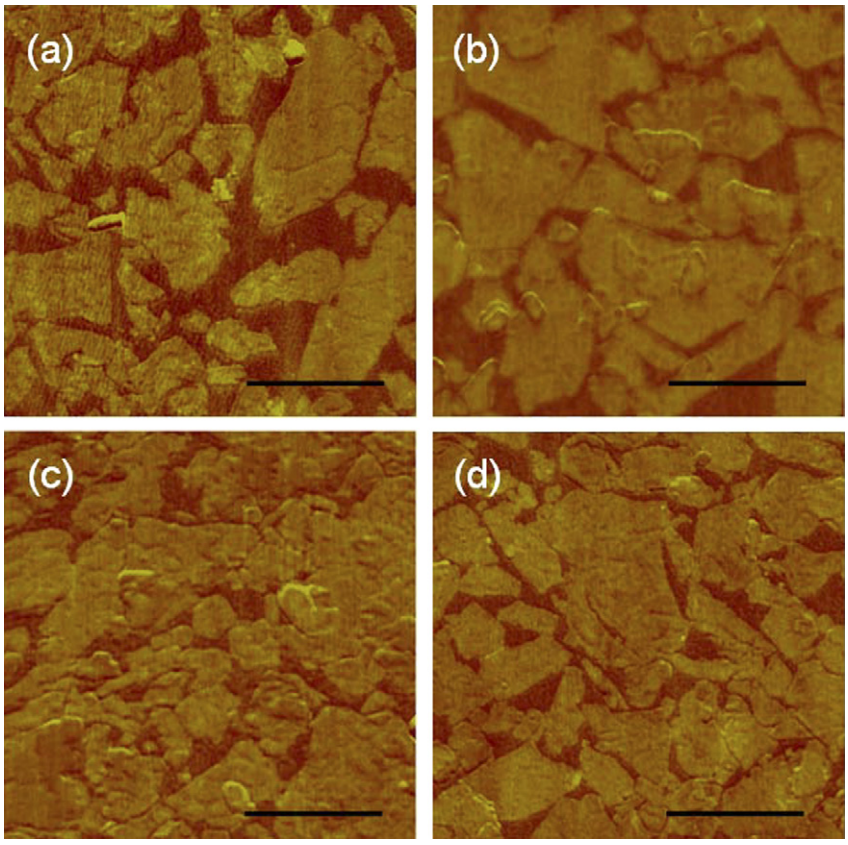

Fig. 6. AFM phase images of (a) C6A ($\pi = 18$ mN/m), (b) C10A ($\pi = 20$ mN/m), (c) C15A ($\pi = 20$ mN/m), and (d) C20A ($\pi = 20$ mN/m) on silicon wafers. (The scale bars correspond to 0.5 μm.)

oclays increase in the order of C6A > C15A > C20A which is consistent with our results in terms of the surfactant coverage. They also calculated the packing density of the surfactant monolayer on the clay surface from $D_s = f_c h_s d N_A/m$, where f_c is the fractional surfactant coverage on the clay, h_s is the thickness of the surfactant layer, $N_A = 6.02 \times 10^{23}$ mol^{-1}, $m = 368$ g/mol and $d = 8.7 \times 10^{-22}$ g/nm^3 are the Avogadro number, the molecular weight and the density of the surfactant, respectively. They found that D_s for fully exchanged system is about 0.8 molecules/nm^2, which corresponds to a loosely packed monolayer of the surfactant on clay surface. From our XR result, however, D_s for C6A, C15A, and C20A are calculated to be 1.4, 1.3, and 1.1 molecules/nm^2, respectively, which are higher than that obtained from CEC for this clay. These results indicate that surfactants not only interact with anionic functional sites on the clay surface, but also they have strong interatomic interactions between the long hydrocarbon alkyl chains, resulting in the formation of the dense layer of ordered molecules with the tilt angle of $35° \pm 6°$ as shown as the inset in Fig. 4.

In addition, it is interesting to note that the coverage of the bottom 2M2HT layer is higher than that of the top 2M2HT layer while its thickness is smaller than the top layer. This tendency is ascribed to the compactness of the surfactant layer on the substrate. The grafting density is not high and hence the layer is compressible once the water is removed. The clay interacts favorably with the silicon oxide surface, compressing the incomplete layer of carbon chains in between. More interestingly, the coverage of the bottom surfactant layer is more than 100%, indicating that some surfactants are not bound to the clay surface and these free surfactants would be also adsorbed onto the Si substrate as illustrated in the inset of Fig. 4 where the surfactant with the blue chains corresponds to an unbounded surfactant. However, we cannot prove the existence of free surfactant at the air/water interface from *in situ* data since free surfactant/water contrast is much lower than the clay/surfactant contrast.

In case of the C10A, we find that the coverage of surfactants is much lower than other clays according to both X-ray reflectivity and AFM results, even though the surfactant concentration is as high as about 125 meq/100 g (see Table 2). This indicates that a large amount of 2MBHT surfactants are unbound to the clay surface and a considerable area of hydrophilic MMT surfaces is exposed. Therefore, we can always tailor the clays to match the blends and obtain optimal surface activity of the clays.

To obtain the surface coverage of the clay at the air/water interface, we assumed that the water occupies the vacant space between the particles and the hydrophilic clay layer sinks below water surface level as illustrated in the inset in Fig. 2. The electron density of the clay layer in the water, $\rho_{\text{clay/water}}$, can be then expressed by

$$\rho_{\text{clay/water}} = \rho_{\text{clay}} C_{\text{clay}} + \rho_{\text{water}}(1 - C_{\text{clay}}), \quad (1)$$

where ρ_{clay} and ρ_{water} represent the electron density of bulk clay and water, respectively. From the equation, we could obtain the clay surface coverage (C_{clay}) of 0.79 which is nicely consistent with the result of dry C15A on the silicon wafer. For the bottom surfactant layer, the surface coverage can be similarly calculated from substitution of the coverage and electron density of surfactants for those of clays in Eq. (1). The coverage of the top surfactant layer was also obtained in the same way, but ρ_{water} was replaced with the electron density of air (ρ_{water}). From the results, we find that the coverage of the surfactant on the clay is 0.82 ± 0.04 (corresponding to 1.2 molecules/nm^2 of surfactant packing density) which is close to that of the dry C15A film.

The implication of these data is that in all cases the coverage of the clay platelet surfaces by the surfactants is incomplete, or each particle contains both polar and non-polar areas. This property is similar to that in surfactant molecules which also contain both hydrophilic (polar) and hydrophobic (non-polar) segments. Hence, organoclays may be able to act as powerful surfactants when mixed with highly immiscible blends of polar and non-polar polymers. This property was recently demonstrated by Si et al. [10] where they showed that the clay platelets were localized at the interfaces between immiscible polymers, partially compatibilizing the blends. The interfacial activity of the clays was postulated to be caused by the formation of *in situ* grafts where both polar and non-polar polymer could be adsorbed onto the corresponding areas on the clay platelet surfaces. Here we provide an experimental justification for this assumption and based on our data we can even calculate the relative ratio of the polar and non-polar polymers that could be adsorbed.

4. Conclusion

In summary, we have shown that X-ray reflectivity is an effective method for accurately determining the degree of the surfactant coverage and the structure of the surfactant molecules on organoclays. We determined that the surfactant coverage was in fact 90, 86, 73, and 0.19% for C6A, C15A, C20A, and C10A, respectively, whereas the CEC value was 52%. Furthermore, we also found that in the covered regions, the surfactant molecules were densely packed and highly ordered in a with a tilt angle of $35^\circ \pm 6^\circ$. From this data, we concluded that the surfactant layer consisted of dense hydrophobic patchy areas, interspersed with polar bare regions, rather than being distributed as a low density, but uniformly hydrophobic surfactant film. This has several important implications on the interaction of the clay platelets when they are dispersed within a polymer blend. In contrast to expectations, that decreasing the surfactant coverage would allow the clays to disperse in polymers of varying polarity, we found that all clays, except the most polar (10A) were easily dispersed within slightly polar homopolymers, such as EVA and PMMA [22–25]. On the other hand, when highly immiscible blends were formed between polar and non-polar polymers, Si et al. [10] reported that these clays were non-specific compatibilizers of a large class of blends. They postulated that this must be due to a patchy, rather than a uniform type of surfactant coverage, where both polar and non-polar polymer could adsorb onto the clay surface forming *in situ* grafts. These grafts would then, as reported in Ref. [10], be highly localized at the interfaces between the polymer domains, thereby decreasing the interfacial tension. The results reported here unambiguously confirm this hypothesis.

Acknowledgment

Support of this work by the NSF-MRSEC is gratefully acknowledged.

References

[1] R.A. Vaia, R.K. Teukolsky, E.P. Giannelis, Chem. Mater. 6 (1994) 1017.
[2] W. Xie, Z.M. Gao, W.P. Pan, D. Hunter, A. Singh, R. Vaia, Chem. Mater. 13 (2001) 2979.
[3] J.W. Lee, Y.T. Lim, O.O. Park, Polym. Bull. 45 (2000) 191.
[4] E. Haokett, E. Manias, E.P. Giannelis, J. Chem. Phys. 108 (1998) 7410.
[5] M. Si, J. Hefter, A. Song, M.H. Rafailovich, J.C. Sokolov, J. Adhesion Sci. Technol. 19 (2005) 1459.
[6] M.Y. Gelfer, C. Burger, B. Chu, B.S. Hsiao, A.D. Drozdov, M. Si, M. Rafailovich, B.B. Sauer, J.W. Gilman, Macromolecules 38 (2005) 3765.
[7] X. Wang, Y. Gao, K. Mao, G. Xue, T. Chen, J. Zhu, B. Li, P. Sun, Q. Jin, D. Ding, Macromolecules 39 (2006) 6653.
[8] X. Li, T. Kang, W.-J. Cho, J.-K. Lee, C.-S. Ha, Macromol. Rapid Commun. 22 (2001) 1306.
[9] B.B. Khatua, D.J. Lee, H.Y. Kim, J.K. Kim, Macromolecules 37 (2004) 2454.
[10] M. Si, T. Araki, H. Ade, A.L.D. Kilcoyne, R. Fisher, J.C. Sokolov, M.H. Rafailovich, Macromolecules 39 (2006) 4793.
[11] M. Gelfer, C. Burger, A. Fadeev, I. Sics, B. Chu, B.S. Hsiao, A. Heintz, K. Kojo, S.-L. Hsu, M. Si, M. Rafailovich, Langmuir 20 (2004) 3746.
[12] K. Shin, Y. Zhang, H. White, M.H. Rafailovich, J. Sokolov, D. Peiffer, Mater. Res. Soc. Symp. (2001) KK8.4.Y.N.A.
[13] N.A. Kotov, F.C. Meldrum, J.H. Fendler, E. Tombácz, I. Dékány, Langmuir 10 (1994) 3797.
[14] R.H.A. Ras, J. Németh, C.T. Johnston, E. DiMasi, I. Dékány, R.A. Schoonheydt, Phys. Chem. Chem. Phys. 6 (2004) 4174.
[15] Y. Umemura, A. Yamagishi, R. Schoonheydt, A. Persoons, F. Schryver, Langmuir 17 (2001) 449.
[16] T.P. Russell, Mater. Sci. Rep. 5 (1990) 171.
[17] M. Tolan, X-Ray Scattering from Soft-Matter Thin Films, Springer, Germany, 1999.
[18] Y. Zhang, Ph.D. thesis, SUNY at Stony Brook, 2000.
[19] H.J. Ploehn, C. Liu, Ind. Eng. Chem. Res. 46 (2006) 7025.
[20] N. Guven, Rev. Mineral. 19 (1998) 497.
[21] http://www.nanoclay.com.
[22] M. Si, M. Goldman, G. Rudomen, M.Y. Gelfer, J.C. Sokolov, M.H. Rafailovich, Macromol. Mater. Eng. 291 (2006) 602.
[23] X. Hu, W. Zhang, M. Si, M. Gelfer, B. Hsiao, M. Rafailovich, J. Sokolov, V. Zaitsev, S. Schwarz, Macromolecules 36 (2003) 823.
[24] M.Y. Gelfer, H.H. Song, L. Liu, B.S. Hsiao, B. Chu, M. Rafailovich, M. Si, V. Zaitsev, J. Polym. Sci. B Polym. Phys. 41 (2002) 44.
[25] M. Gelfer, C. Avila-orta, L. Liu, L. Yang, B. Chu, B.S. Hsiao, H.H. Song, M. Si, M. Rafailovich, A.H. Tsou, Polym. Eng. Sci. 42 (2004) 1841.